Diagn Interv Radiol 2021; 27: 7–14

ABDOMINAL IMAGING

ORIGINAL ARTICLE

MRI quantification techniques in fatty liver: the diagnostic performance of hepatic T1, T2, and stiffness measurements in relation to the proton density fat fraction

Ayşe Erden
Diğdem Kuru Öz
Elif Peker
Melahat Kul
Funda Seher Özalp Ateş
İlhan Erden
Ramazan İdilman

PURPOSE
Nonalcoholic fatty liver disease (NAFLD) can progress to liver cirrhosis and is predicted to become the most frequent indication for liver transplantation in the near future. Noninvasive assessment of NAFLD is important for diagnosis and patient management. This study aims to prospectively determine the liver stiffness and T1 and T2 values in patients with NAFLD and to compare the diagnostic performance of magnetic resonance elastography (MRE) and mapping techniques in relation to the proton density fat fraction (PDFF).

METHODS
Eighty-three patients with NAFLD and 26 participants with normal livers were imaged with a 1.5 T scanner. PDFF measurements obtained from the multiecho Dixon technique were used to quantify the liver fat. MRE, native T1 mapping (modified Look-Locker inversion recovery [MOLLI] schemes 5(3)3, 3(3)3(3)5, and 3(2)3(2)5 and the B1-corrected variable flip angle [VFA] method), and T2 mapping values were correlated with PDFF. The diagnostic performance of MRE and the mapping techniques were analyzed and compared.

RESULTS
T1 values measured with the MOLLI schemes and the B1-corrected VFA ($p < 0.001$), and the stiffness values from MRE ($p = 0.047$) were significantly higher in the NAFLD group. No significant difference was found between the groups in terms of T2 values ($p = 0.127$). In differentiation of the NAFLD and control groups, the B1-corrected VFA technique had slightly higher accuracy and area under the curve (AUC) than the MOLLI schemes. In the NAFLD group, there was a good correlation between the PDFF, MOLLI 3(3)3(3)5 and 3(2)3(2)5, and VFA T1 measurements (r=0.732; r=0.735; r=0.716, $p < 0.001$, respectively).

CONCLUSION
Liver T1 mapping techniques have the potential to distinguish steatotic from nonsteatotic livers, and T1 values seem to have a strong correlation with the liver fat content.

Nonalcoholic fatty liver disease (NAFLD) is one of the most common causes of chronic liver disease, with an estimated worldwide prevalence of around 25% (1). It may range from simple steatosis, which is considered a benign condition, to nonalcoholic steatohepatitis (NASH), which can progress to fibrosis, cirrhosis, liver failure, and hepatocellular carcinoma. NAFLD is also known to be associated with metabolic syndrome, which is a risk factor for cardiovascular disease and type II diabetes mellitus (2–4).

The gold standard method for diagnosing NAFLD and distinguishing its different patterns is a liver biopsy which has considerable limitations, including sampling errors, its invasive nature and associated complication risks, small sample size, and inter- and intraobserver variability (5, 6). These drawbacks constrain its utility for clinical monitoring and make it unsuitable as a screening method. Therefore, there is an urgent clinical need for an accurate noninvasive approach in the assessment of NAFLD. Accordingly, both the European Association for the Study of the Liver and the American Association for the Study of Liver Disease propose magnetic resonance imaging (MRI) as a noninvasive diagnostic tool for NAFLD (7, 8). Proton density fat fraction (PDFF)-based MRI and magnetic resonance spectroscopy (MRS) techniques are considered the most accurate noninvasive methods for the quantification of liver fat (9–12). The PDFF is accepted as a standardized biomarker of hepatic steatosis. Stud-

From the Departments of Radiology (A.E., D.K.Ö. ✉ *digdem_k@hotmail.com*, E.P., M.K., İ.E.), Biostatistics (F.S.Ö.A.), and Gastroenterology (R.İ.), Ankara University School of Medicine, Ankara, Turkey.

Received 16 December 2019; revision requested 05 January 2020; last revision received 22 March 2020; accepted 05 April 2020.

Published online 3 December 2020.

DOI 10.5152/dir.2020.19654

You may cite this article as: Erden A, Kuru Öz D, Peker E, et al. MRI quantification techniques in fatty liver: the diagnostic performance of hepatic T1, T2, and stiffness measurements in relation to the proton density fat fraction. Diagn Interv Radiol 2021; 27: 7–14

ies suggest that this biomarker is equivalent to the hepatic "signal fat fraction" (FF) after correcting all the confounding factors (13). However, PDFF measurement is not suitable for the assessment of any inflammation or fibrosis in NAFLD (13). On the other hand, recent studies have shown that other quantitative MRI techniques such as magnetic resonance elastography (MRE) and T1–T2 mapping can be useful in detecting hepatic inflammatory and fibrotic changes (14, 15–21). Thus, the application of a multiparametric MRI protocol might be helpful in liver tissue characterization and thereby in the risk stratification and therapeutic management of patients with NAFLD.

In this prospective study, we aimed to determine liver stiffness and T1 and T2 values in patients with NAFLD and nonsteatotic subjects and compare the diagnostic performance of MRE and mapping techniques in relation to the FF.

Methods

Subjects

Our institutional human research ethics committee approved this prospective study (I2-51-19). All participants gave written informed consent prior to the examination. Overall, 273 consecutive subjects who underwent multiparametric liver imaging with findings of fatty liver on ultrasonography (US) between November 2017 and May 2019 were eligible for the study. The US findings were used only to determine patients' eligibility for the study. Of these patients, 164 were excluded due to the following reasons: (a) chronic liver disease such as hepatitis B and C, primary biliary cirrhosis, Wilson disease, alcoholic hepatitis, and autoimmune hepatitis (n=105); (b) hepatic iron overload on multiecho Dixon sequence (n=3); (c) technically suboptimal imaging due to motion artifacts, obesity, or fat-water swaps (n=7); (d) large focal lesions and diffuse or multifocal liver lesions (n=4); (e) obstructive biliary dilatation (n=25); and (f) hepatic congestion/vascular occlusion (n=6) or incomplete examination due to patient intolerance (n=3). Eleven patients with NAFLD who had morphologic signs of chronic liver disease on standard MRI were also excluded, since advanced fibrosis causes the reduction of hepatocytes by volume, leading to an apparent reduction in liver fat (22).

Finally, 83 patients comprised the study population. The steatosis grading was performed according to the PDFF values. Out of 273 subjects, 11 healthy volunteers who were willing to take part in the study and 15 participants suspected of fatty liver during US but with no fat accumulation on MRI formed the control group.

Main points

- T1 mapping can potentially be used to differentiate patients with NAFLD from normal subjects.
- T1 values seem to have a strong correlation with liver fat content.
- MRE can be used to assess inflammation and/or fibrosis in patients with NAFLD.

MRI technique

The subjects were imaged with a 1.5 T scanner (Aera, Siemens Medical Systems) equipped with an 18-channel body matrix coil and a 32-channel spine matrix coil, of which 8 were used. After obtaining sequences in the standard liver MRI protocol (coronal T2-weighted HASTE, transverse T2-weighted BLADE, transverse T2-weighted fat-suppressed BLADE, diffusion-weighted imaging with echo-planar imaging and b values of 50, 400, and 800 s/mm^2, and T1 volumetric interpolated breath-hold examination [VIBE] e-Dixon), the sequences that provide parametric maps for the quantification of hepatic fat, iron, stiffness, and T1 and T2 relaxation times were acquired. The vendor-supplied package (LiverLab), which offers the evaluation and quantification of fat and iron, was used. LiverLab consisted of three sequences incorporated into the abdomen protocol. T1 VIBE e-Dixon, VIBE q-Dixon (a single breath-hold multiecho Dixon sequence with six echoes that provides volumetric FF and R2* maps), and HISTO (15-second breath-hold single-voxel STEAM spectroscopy with a 3×3×3 cm^3 voxel size) sequences were performed in conjunction with a routine liver examination. The R2* values were corrected for fat effects, and the fat percentage was corrected for the T2* effects using the scanner's software.

MRE

For MRE, a wave motion-sensitized phase-contrast two-dimensional gradient echo sequence was used to track shear waves and produce raw data. Four 10 mm thick slices were obtained through the largest cross-section of the liver, with breath-holds in end-expiration. Elastograms, wave images, and confidence maps were then reconstructed using dedicated postprocessing software. The scanning time of each transverse slice was 17 seconds. The MRE was completed in about 2 minutes together with four breath-holds and resting periods.

T1 mapping

A modified Look-Locker inversion recovery (MOLLI) approach was used for the native T1 mapping utilizing a single breath-hold, a balanced steady-state free precession (bSSFP) sequence with electrocardiography-gated 5(3)3, (3)3(3)5, and 3(2)3(2)5, and heart rate corrected (hrc)5(3)3 sampling schemes, as previously described (23–25).

The T1 maps were acquired in a single transverse plane with a slice thickness of 10 mm. The hepatic level of T1 map section was chosen from the MRE confidence maps with the largest area for the stiffness measurement. In addition, a B1 inhomogeneity-corrected volumetric T1 map with a variable flip angle (VFA) method was obtained for each patient. Because VFA techniques are intrinsically sensitive to the inhomogeneities of the transmitted RF field, B1 corrections were implemented to improve the acquired T1 maps' spatial homogeneity. A VIBE sequence was used to achieve volumetric coverage of the liver in the VFA method. Multisection data (72 slices) were acquired with a breath-hold of 19 seconds. Inline T1 maps were constructed at the scanner using the vendor-supplied software.

T2 mapping

The T2 mapping was performed using both the fast low-angle shot inversion-recovery gradient echo (FLASH) and balanced steady-state free precession (True FISP) sequences with a slice thickness of 10 mm. Cardiac gating was used to time the image acquisition. Each slice had the same transverse anatomic level as in the T1 mapping.

The detailed sequence-specific parameters of the MRE and T1 (MOLLI sampling schemes and B1-corrected VFA T1 map) and T2 (FLASH and True FISP) mapping techniques can be found in Table 1.

MRI analysis

In the present study, the PDFF was accepted as a standardized biomarker of hepatic steatosis, and the complex-based fat quantification (multiecho Dixon) method was accepted as the reference standard for

Table 1. Pulse sequence parameters of MRE, T1 and T2 mapping at 1.5 T imager

Parameter	MRE	MOLLI 5(3)3[b]	MOLLI 3(3)3(3)5	MOLLI 3(2)3(2)5	VFA T1 map VIBE (3D)	T2 FLASH	T2 TrueFISP
Matrix size	48×128	144×256	180×224	180×224	156×256	116×192	116×192
Slice thickness (mm)	10	10	10	10	3.5	10	10
Distance factor %	-	-	-	-	20	-	-
Repetition time (ms)	50	279	419	419	4.3	207	193
Echo time (ms)	27.5	1.12	1.64	1.64	2.08	1.06	2.08
Inversion time (ms)	-	180	260	260		-	-
Flip angle (degrees)	25	35	50	50	3 and 15	12	70
Reduction factor[a]	2	2	2	2	2	2	2
Averages	1	1	1	1	3	1	1
FoV (mm)	400×300	360×306	390×313	390×313	380×309	360×289	360×289
Orientation	Transverse	Transverse	Transverse	Transverse	Transverse	Transverse	Transverse
Cardiac gating	No	Yes	Yes	Yes	No	Yes	Yes
Bandwidth (Hz/Px)	250	1085	603	603	350	1184	1184
Acquisition time (s)	17 (17×4=68)	8–15[c]	12–15[c]	10–20[c]	19	7–12[c]	12[c]

MRE, magnetic resonance elastography; MOLLI, modified Look-Locker inversion recovery; VFA, variable flip angle; VIBE, volumetric interpolated breath-hold examination; 3D, three-dimensional; FLASH, fast low-angle shot; FISP, fast imaging with steady precession; FoV, field of view.
[a]Parallel acquisition technique GRAPPA (GeneRalized Autocalibrating Partial Parallel Acquisition) was used for all sequences except for VIBE (3D) T1 map in which CAIPIRINHA (Controlled Aliasing In Parallel Imaging Results IN Higher Acceleration) technique was used.
[b]The parameters for heart rate corrected MOLLI 5(3)3 scheme is identical with MOLLI 5(3)3 scheme.
[c]Acquisition time depends on heart rate.

steatosis diagnosis. Although MRS is known as the most accurate method for fat quantification (13, 26), only the measurements obtained from the parametric FF maps provided by the multiecho Dixon sequence were used to quantify fat in this study. The reason behind not using the MRS results for the statistical analysis was that only a limited area (27 cm^3 voxel in the right lobe) can be evaluated using this technique. The PDFF values measured from the parametric FF maps are known to be closely correlated with the MRS analysis (13, 26). Thus, the MRS results were used only to crosscheck the PDFF results.

The PDFF measurements were done on the parametric FF maps by a radiologist with 20 years of experience in abdominal MRI, who was blinded to the patients' clinical histories. For quantification of the hepatic FF, three ovoid region of interests (ROI) of approximately 200–300 mm^2 were placed within the mid-right hepatic lobe on the parametric FF map generated on MRI system console. The ROIs were drawn on three transverse sections and included as much of the liver parenchyma as possible, excluding large vessels, bile ducts, liver edges, and artifacts. The PDFF values for each ROI were recorded and averaged to obtain a mean value for each patient. An FF threshold of 6.3% was accepted as the upper normal limit. The hepatosteatosis grading (grade 1 or mild, 6.4%–17.4%; grade 2 or moderate, 17.4%–22.1%; and grade 3 or severe, ≥22.1%) was done using the PDFF results. These PDFF thresholds were based on a study from the NASH Clinical Research Network (10, 27).

All images were transferred to a dedicated workstation (Syngo.via, Siemens Healthcare) for further analysis. The values measured from the confidence maps of the MRE and T1 and T2 parametric maps were reported as a single consensus reading of two radiologists with 3 and 8 years of experience in abdominal MRI. The readers were blinded to the patients' PDFF values and clinical histories. Liver stiffness values in kilopascals (kPa) were obtained by drawing a freehand ROI, avoiding the margins of the liver (artifactual "hot spot" areas) and major vessels on the confidence map. The liver stiffness values for each MRE examination were expressed as a mean of the mean stiffness measurements from each of the four transverse sections through the mid-liver.

The T1 and T2 liver values were measured directly on pixel-based color maps derived from MOLLI and FLASH/TrueFISP image sets, respectively. A single section of the liver analyses was performed by manually drawing a ROI just inside liver's outer margins, outlining the entire cross-sectional area, excluding major vessels (Fig. 1). The measurements were repeated twice, and the average value (in ms) was used for analysis. The T1 values on the VFA T1 maps passing from the same level as in the MOLLI sequences were also measured by drawing a freehand ROI along the liver's margins, avoiding major vessels.

Liver biopsy

Liver biopsy was available in 44 patients. In 29 patients, the time interval between the liver biopsy and MRI was less than six months (mean, 88 days; range, 0–178 days). A subgroup with a biopsy was formed to analyze the effects of fat, inflammation, and fibrosis on multiparametric imaging. The results of all biopsies have been included for this analysis, irrespective of their length or duration.

Statistical analysis

All statistical analyses were performed using SPSS for Windows, version 11.5 (SPSS Inc.). A Shapiro–Wilk test was used to assess the assumption of normality. Normally distributed continuous variables (only age) were expressed as mean ± standard deviation, while the continuous variables that

Table 2. Comparison of quantitative parameters of MRE and T1 in patients and controls

Sequences*	Controls Median (min–max)	Patients Median (min–max)	*p*
MRE (kPa)	2.13 (1.57–2.84)	2.40 (1.40–4.25)	0.047
MOLLI 5(3)3	564.8 (445.4–605.4)	656.2 (502.9–1028.1)	<0.001
MOLLI 3(3)3(3)5	595.6 (457.6–644.6)	766.2 (561.2–2210.2)	<0.001
MOLLI 3(2)3(2)5	582.2 (464.0–637.4)	744.6 (538.5–2221.5)	<0.001
MOLLI $5(3)3_{hrc}$	556.8 (442.1–465.6)	638.3 (465.6–931.1)	<0.001
B1 corrected VFA	690.9 (505.6–761.3)	929.4 (691.4–1529.6)	<0.001
T2 FLASH	41.4 (34.0–44.8)	42.0 (33.2–44.1)	0.127
T2 TrueFISP	49.1 (45.1–53.1)	49.5 (39.4–55.1)	0.679

MRE, magnetic resonance elastography; MOLLI, modified Look-Locker inversion recovery; VFA, variable flip angle; hrc, heart rate corrected; FLASH, fast low-angle shot; FISP, fast imaging with steady precession.
*T1 and T2 values are in ms.

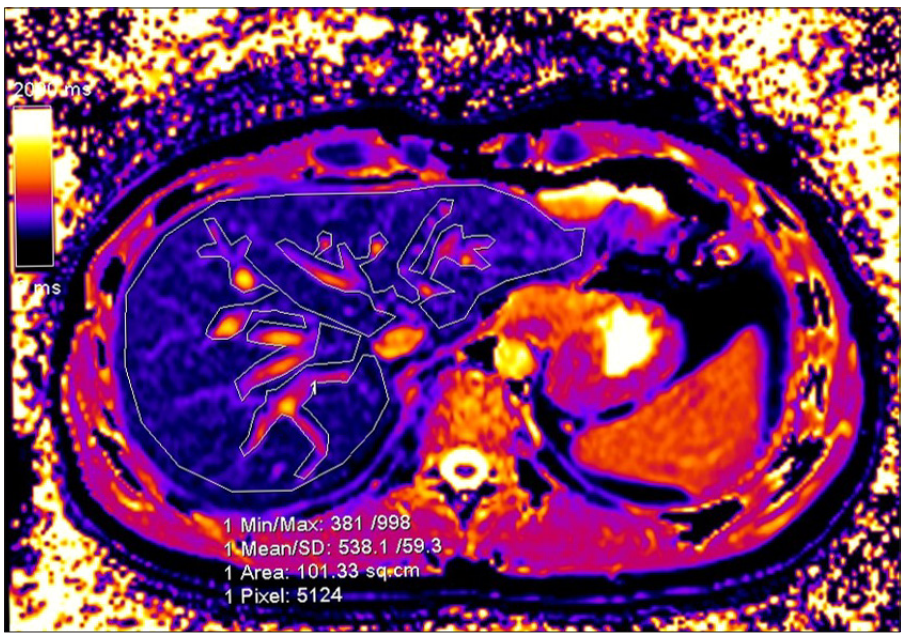

Figure 1. A 28-year-old man with normal liver. T1 relaxation time of the liver was determined by manually drawing a ROI just inside the outer margins of the liver, outlining the entire cross-sectional area, excluding major vessels.

did not have a normal distribution (MRE, T1 MOLLI mapping schemes, T2 mapping, and B1-corrected VFA T1 mapping) were expressed as a median (minimum-maximum). Also, the categorical variables (e.g., sex) were summarized as counts (percentages). For the MRE, T1 MOLLI mapping schemes, T2 mapping, and B1-corrected VFA T1 mapping, the differences between the groups were tested using a Mann-Whitney U-test. Associations between the groups (patients-control) and sex were determined using Pearson chi-square analysis, and the associations between the PDFF values and MRE, T1 mapping, and T2 mapping were determined using Spearman's correlation coefficient.

The diagnostic performance of the MRE, T1 MOLLI mapping schemes, and B1-corrected volumetric VFA T1 mapping was tested using the area under the curve (AUC), sensitivity, specificity, and accuracy in predicting the presence of fat and grading steatosis.

The level of interobserver agreement was assessed using kappa statistics. A two-sided *p* value <0.05 was considered statistically significant.

To examine the effects of fat, inflammation, and fibrosis on the MRE, T1 MOLLI mapping schemes, and B1-corrected VFA T1 mapping, a simple linear regression analysis was used. The variables, which had a significance level of $p < 0.20$ from the simple linear regression analysis, were identified as candidate variables for the multivariable model.

Results

Eighty-three patients with NAFLD were included in this prospective study (mean age, 52.5±9.4 years; range, 31–71 years). Sixty-two (74.7%) of the patients were female, and 21 (25.3%) were male. Out of these, 61 (73.5%) patients had grade 1 (mild), 10 (12%) had grade 2 (moderate) and 12 (14.5%) had grade 3 (severe) steatosis according to PDFF values. The control group composed of 26 participants (mean age, 47.3±12.6 years; range, 21–69 years) without any laboratory and clinical findings indicative of any liver disease. Fourteen participants (53.8%) in the control group were female, and 12 participants (46.2%) were male. The patients and the controls were similar with respect to gender ($p = 0.043$) but different with respect to age ($p = 0.026$).

The median (minimum-maximum) MRE, T2, and T1 (including all MOLLI sequences and B1-corrected VFA techniques) values are shown in Table 2. The T1 values were obtained using both mapping techniques, and the stiffness values were significantly higher in the NAFLD group ($p < 0.001$). No significant difference was found between the groups in terms of T2 values ($p = 0.127$). The stiffness values from the MRE were significantly higher in the NAFLD group ($p = 0.047$). The T1 mapping technique with the highest accuracy and AUC was B1-corrected VFA. The cutoff values, AUC, sensitivity, specificity, and accuracy with 95% confidence intervals in differentiating the NAFLD and control groups' MRE, MOLLI 5(3)3, MOLLI 3(3)3(3)5, MOLLI 3(2)3(2)5, and hrc-5(3)3, and B1-corrected VFA map are shown in Table 3.

In the NAFLD group, there was a good correlation between the PDFF and T1 values obtained with MOLLI 3(3)3(3)5, MOLLI 3(2)3(2)5, and the B1-corrected VFA T1 maps (r=0.732, $p < 0.001$; r=0.735, $p < 0.001$; r=0.716, $p < 0.001$, respectively) (Fig. 2). Even though there was also a correlation between the MOLLI 5(3)3 sequence and the PDFF values, this proved to be weak (r=0.342, $p = 0.002$). The MRE, T1 values of the hrc-MOLLI 5(3)3 sequence, and T2 values (T2 FLASH and T2 True FISP) were not correlated with the PDFF (r=-0.168,

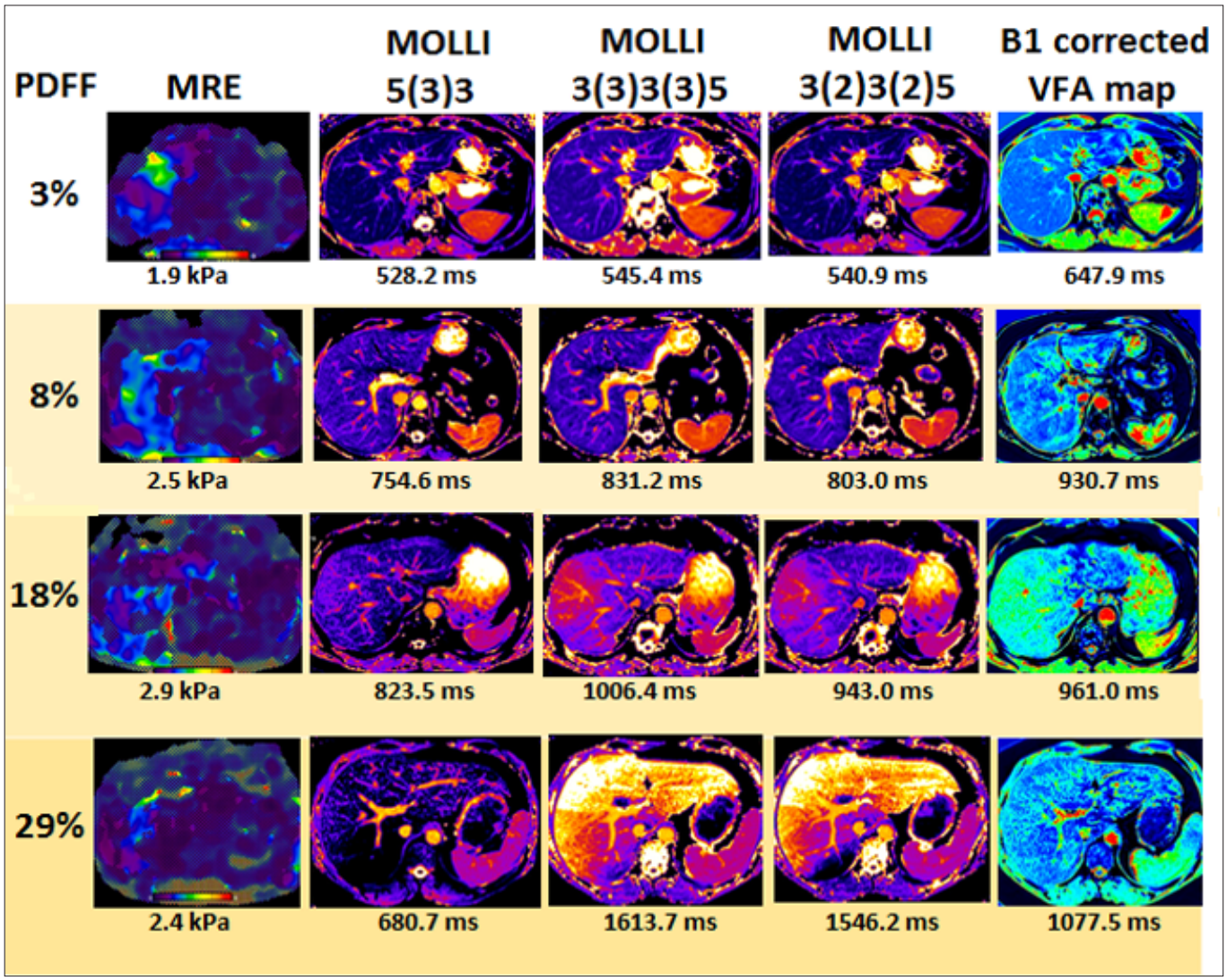

Figure 2. A 55-year-old woman, a 49-year-old woman, a 44-year-old man, and a 36-year-old woman with proton density fat fraction (PDFF) 3%, 8%, 18%, and 29%, respectively. Magnetic resonance elastography-assessed liver stiffness values measured from confidence map and T1 values obtained with MOLLI 5(3)3, MOLLI 3(3)3(3)5, MOLLI 3(2)3(2)5 sampling schemes, and B1-corrected VFA T1 map are shown in corresponding rows. Note that T1 values correlate well with the percentage of liver PDFF.

Table 3. The cutoff values, AUC, sensitivity, specificity and accuracy with 95% CI in differentiating NAFLD and control group

	Cutoff (ms)	AUC	Accuracy % (95% CI)	Sensitivity % (95% CI)	Specificity % (95% CI)	*p*
MRE (kPa)	2.9	0.634	41.3 (31.9–50.8)	23.8 (15.8–34.1)	100 (86.2–100)	0.047
MOLLI 5(3)3	605.9	0.879	79.6 (72.0–87.2)	73.2 (62.7–81.6)	100 (87.1–100)	<0.001
3(3)3(3)5	646.1	0.976	94.5 (90.2–98.8)	92.8 (85.1–96.6)	100 (87.1–100)	<0.001
3(2)3(2)5	638.4	0.973	93.6 (89.0–98.2)	91.6 (83.6–95.9),	100 (87.1–100)	<0.001
hrc-5(3)3	606.6	0.821	70.6 (62.1–79.2)	61.5 (50.7–71.2),	100 (87.1–100)	<0.001
B1-corrected VFA	741.5	0.991	97.9 (95.0–100)	98.7 (92.8–99.8),	95 (76.4–99.1)	<0.001

AUC, area under the curve; CI, confidence interval; MRE, magnetic resonance elastography; MOLLI, modified Look-Locker inversion recovery; hrc, heart rate corrected; VFA, variable flip angle.

p = 0.137; r=0.128, p = 0.248; r=-0.210, p = 0.056; r=-0.101, p = 0.363, respectively).

The results of the ROC analysis performed in the NAFLD group to determine the effectiveness of the MOLLI sequence schemes and the B1-corrected VFA T1 map in differentiating mild steatosis from moderate/severe steatosis and severe steatosis from mild/moderate steatosis are outlined in Tables 4 and 5. The MOLLI 3(3)3(3)5 and 3(2)3(2)5 sequences seem to be slightly better than B1-corrected VFA mapping in differentiating both mild from moderate/severe steatosis and severe from mild/moderate steatosis.

The kappa values for the interobserver agreement in the T1 values for the MOLLI 5(3)3, 3(3)3(3)5, 3(2)3(2)5, and hrc-5(3)3 and the B1-corrected VFA T1 map were 0.98, 0.99, 0.99, 0.97, and 0.97, respectively; $p < 0.001$ for all.

All 44 patients with liver biopsies had histologic findings suggestive of steato-

Table 4. Results of ROC analysis of T1 mapping in differentiating mild steatosis from moderate/severe steatosis

	Cutoff (ms)	AUC	*p*	Accuracy % (95% CI)	Sensitivity % (95% CI)	Specificity % (95% CI)
MOLLI schemes						
MOLLI 5(3)3	741.8	0.722	0.003	79.5 (70.5–88.5)	50.0 (29.9–70.1)	89.7 (79.2–95.2)
3(3)3(3)5	887.3	0.897	<0.001	92.4 (86.6–98.3)	81.0 (60.0–92.3)	96.6 (88.3–99.1)
3(2)3(2)5	861.6	0.912	<0.001	92.4 (86.6–98.3)	81.0 (60.0–92.3)	96.6 (88.3–99.1)
B1-corrected VFA	960.5	0.868	<0.001	83.1 (74.4–91.8)	94.4 (74.2–99.0)	79.3 (66.5–88.0)

ROC, receiver operating characteristics; AUC, area under the curve; CI, confidence interval; MOLLI, modified Look-Locker inversion recovery; VFA, variable flip angle.

Table 5. Results of ROC analysis of T1 mapping in differentiating severe steatosis from mild/moderate steatosis

	Cutoff (ms)	AUC	*p*	Accuracy % (95% CI)	Sensitivity % (95% CI)	Specificity % (95% CI)
MOLLI schemes						
MOLLI 5(3)3	781.8	0.820	0.001	85.9 (78.2–93.8)	72.7 (43.4–90.3)	88.1 (78.2–93.8)
3(3)3(3)5	1022.4	0.995	<0.001	98.7 (96.3–100)	100 (74.2–100)	98.5 (92.1–99.7)
3(2)3(2)5	917.9	0.992	<0.001	94.9 (90.1–99.8)	100 (74.1–100)	94.1 (85.8–97.7)
B1-corrected VFA	1076.1	0.938	<0.001	93.0 (87.0–98.9)	100 (72.3–100)	91.8 (82.2–96.5)

ROC, receiver operating characteristics; AUC, area under the curve; CI, confidence interval; MOLLI, modified Look-Locker inversion recovery; VFA, variable flip angle.

hepatitis, with grade 1 inflammation in 26, grade 2 inflammation in 15, and grade 3 inflammation in 2 patients. In a total of 29 patients, different degrees of fibrotic changes were also present, and a histopathologic analysis showed grade 1 fibrosis in 19, grade 2 fibrosis in 4, and grade 3 fibrosis in 6 patients.

The linear regression analysis revealed that a higher grade of inflammation and fibrosis was associated with slightly higher MRE-assessed stiffness values. An increase in inflammation from histologic grade 1 to grade 3 leads to an increase in liver stiffness by 1 kPa. Histologic hepatic fibrosis grades 2 and 3 increase stiffness by 0.7 and 0.8 kPa, respectively, compared to grade 0 fibrosis. A histologically proven higher steatosis grade correlated with MOLLI sequences 3(3)3(3)5 and 3(2)3(2)5. Relative to grade 1 steatosis, the presence of grade 3 steatosis leads to an increase of 281 ms in the T1 measurement with the MOLLI 3(3)3(3)5 sequence. Histopathological grade 3 steatosis also results in a 306 ms increase in the T1 measurement with the MOLLI 3(2)3(2)5 sequence, relative to grade 1 steatosis. However, according to the multivariable linear regression, these associations were statistically not significant.

Discussion

Although the gold standard for NAFLD assessment is a liver biopsy, its well-known limitations have driven a search for noninvasive screening and risk stratification methods (6). Today, imaging techniques play an important role in the diagnosis and monitoring of NAFLD. US is widely used as a first-line imaging modality for detecting a fatty liver, but the reported accuracy and reliability have been inconsistent across the studies. Computed tomography is also commonly used for the evaluation of NAFLD. The degree of fat deposition can be estimated based on hepatic attenuation values with increasing liver fat content, but the method involves radiation exposure. Currently, MRI is regarded as the most definitive imaging tool to quantitatively evaluate hepatic steatosis. MRS and magnitude- and complex-based fat quantification techniques are three methods that exploit fat-water precession differences to assess NALFD (6–9, 26).

Conversely, liver T1 mapping has shown promise as a noninvasive biomarker of hepatic fibroinflammatory disease (28). Recent studies suggested that hepatic relaxation times are not only influenced by liver fibrosis and inflammation but also by fat in the liver (28–30). The MOLLI approach, which we used for the T1 mapping in our study, was originally developed for cardiac applications. The readout is based on a single-shot bSSFP sequence. The original MOLLI uses a 3(3)3(3)5 scheme, with the numbers outside the parentheses indicating the number of images acquired after each magnetization preparation pulse, and the numbers inside the parentheses indicating the length of the pause separating the image acquisition and any subsequent magnetization preparation pulse. In the original MOLLI 3(3)3(3)5 scheme, 3 inversion pulses are used, and 11 images are obtained in a single breath-hold of 17 heartbeats (about 15 s). A recovery period between the inversion pulses includes 6 heartbeats. In the MOLLI variants, the duration between the prepulses and pauses are changed to reduce the scan time by up to 8–10 seconds (23–25). The 5(3)3 variant, which shifts the 5-beat image acquisition to the beginning, allows more time (8 heartbeats) for the recovery of the longitudinal magnetization (31). This MOLLI scheme has a total scan duration of 11 heartbeats and produces 8 images with varying inversion times. The shorter breath-hold time employed by the 5(3)3 sequence means it can be better tolerated in patients with difficulty holding their breath. The other variant we used in our study was the MOLLI 3(2)3(2)5 scheme. In this implementation, 3 images were acquired after the first and second inversions, and 5 images were acquired after the third inversion, with 2 recovery beats to allow for T1 recovery before the second and third cycles. This MOLLI scheme has a total scan duration of 15 heartbeats and produces 11 images.

The results of the present study indicate that the T1 parameters had very good diagnostic value for the assessment of the presence of steatosis and inflammation/fibrosis in patients with NAFLD. The T1 mapping technique with the highest accuracy and AUC was B1-corrected VFA T1 mapping. Our study also showed that the T1 values obtained by MOLLI 3(3)3(3)5, MOLLI3(2)3(2)5, and the B1-corrected VFA T1 mapping had a strong correlation with the liver PDFF. The MOLLI 3(3)3(3)5 and 3(2)3(2)5 sequences seem to be slightly better than B1-corrected VFA mapping at differentiating both mild from moderate/severe steatosis and severe from mild/moderate steatosis. Interestingly, we observed that in the presence of severe hepatosteatosis, the T1 maps achieved with

MOLLI 3(3)3(3)5, MOLLI3(2)3(2)5, and the B1-corrected VFA technique showed distinct parenchymal heterogeneity visible as grains in the hepatic tissue, which was not seen in normal liver or in lower grades of fatty infiltration.

In our study, the increase in MRE measurements in patients with NAFLD showed not good but sufficient diagnostic accuracy (AUC, 0.634). In the study conducted by Loomba et al. (19), the MRE performance in discriminating NASH from non-NASH was reported to be modest (AUC, 0.73). According to the results of our linear regression analysis, histopathological high-grade inflammation and fibrosis causes a slight increase in MRE stiffness values compared to low grade, while high-grade fat increased the T1 values in MOLLI 3(3)3(3)5 and 3(2)3(2)5) compared to low grade. Even though this finding was statistically not significant, we consider it clinically relevant, as this association corroborates prior study results (17–20). Actually, it is known that fatty infiltration alone does not affect measurements of hepatic stiffness values. However, if the disease progresses to inflammation, the MRE-assessed hepatic stiffness does increase, even before the onset of fibrosis (17, 18, 32). Hardy et al. (33) recommended that MRE be chosen as a second-line investigation for NAFLD staging to identify candidates for liver biopsy.

Our finding of higher T1 values in the NAFLD group compared to the non-NAFLD controls is consistent with the findings of other published studies (28–30). In a recent study using MOLLI design 3(3)5, Obmann et al. (28) reported that T1 mapping allows differentiating between the reference population and patients with steatosis and/or fibrosis. In this study, in steatotic patients with increased liver stiffness on MRE, the T1 relaxation time was significantly longer than in the reference population. In a study reported by Pavlides et al. (14) the T1 values are shown to be correlated with the NAFLD/NASH and fibrosis severity. The elevated T1 in the steatotic liver can be explained by the effects of inflammation and fibrosis dominating the fatty-related T1 decrease. However, recent studies showed the contribution of confounding physical/technical factors in bSSFP mapping methods (MOLLI and saturation recovery single-shot acquisition [SASHA] methods) (34, 35). T1 measurement using these methods assumes a single species (e.g., water or fat) and performs a monoexponential curve fit to derive a single T1 value. The authors also reported that the T1 estimate of combined water and fat varies substantially with the FF. For a low FF, the T1 elevation is approximately linear, with the FF in the range of a low FF. For an FF in the 30%–50% range, the recovery signal model is an extremely poor fit, and the T1 estimate is undefined in this range. The appearance of fatty changes in the T1 map depends on whether the off-resonance creates an in-phase or out-of-phase mixture (34, 35). Such off-resonance effects causing the elevation of T1 values is also referred to in the studies related to fatty liver (28, 29). There are two aspects of this issue to be emphasized. First, an FF greater than 30%–50%, which is problematic in experiments, is very rare in the liver in a real practice setting. Second, the abovementioned dependency of the T1 estimate accuracy can be considered a positive property of MOLLI, as it tends to accentuate liver T1 time differences in normal and steatotic livers. Mozes et al. (30) suggested that the effects of fibroinflammatory changes might be characterized by using short MOLLI scheme 5(1)1(1)1.

T2 mapping has been previously shown to be useful in characterizing both cardiovascular and chronic liver disease, with elevated T2 values in the presence of inflammatory and fibrotic processes (15, 36). However, in our study, there was no statistically significant difference between patient and control groups regarding the T2 values. A reason could be that we used the freehand ROI technique for measurements. Since only major vessels are visible on the T2 map, vessels of smaller caliber could be omitted and might have contributed to the mean T2 relaxation times. This potential problem can be avoided by placing multiple small ROIs on regions definitely identified as hepatic parenchyma through correlation with standard MRI sequences.

This study has several limitations. First, the sample size in the subgroups was relatively small, which may have limited the ability of the analysis to detect subtle effects of inflammation and fibrosis on the quantification techniques. Second, performing PDFF measurements using a single radiologist may be considered a limitation. Third, in nearly half of the patients (n=39), a liver biopsy was not performed, or the time interval between the liver biopsy and MRI was too long (n=15). Therefore, a histopathologic correlation of the MRI results could not be made in all patients. We have created a subgroup consisting of patients whose biopsy was available and have included all biopsies in the final analysis, irrespective of their length. This may have affected the accuracy of the linear regression assessment. A percutaneous liver biopsy, however, is not an ideal reference standard for steatosis, inflammation, or fibrosis. Biopsies can underestimate the degree of these pathologies about 20%–30% of the time because of their patchy distribution in the liver (36). Also, histopathological indices have a wide range of both inter/intraobserver and sampling variations (37). Fourth, the T1 maps with three different MOLLI sampling schemes and the T2 maps assessed in our study covered one large transverse slice. A whole liver evaluation would reduce sampling errors and allow better heterogeneity characterization. Volumetric T1 mapping is suitable for addressing this heterogeneous fatty infiltration limitation, as it provides global information about the liver T1 values in a single breath-hold (38). In our study, further analysis of the whole liver using 3D VFA mapping was also performed. However, for comparison purposes, we measured T1 values only from a slice covering the liver portion identical with that in the MOLLI sequences. Fifth, the MOLLI methods we preferred in the present study are known to be influenced by tissue T2, heart rate, inversion efficiency, and the magnetization transfer effect (39). Because of this dependency, the values we measured are not "true" T1 values but shorter "apparent" T1 values (40). As may be related to the abovementioned factors, we found the T1 measurements on the VFA T1 maps to be higher than those in the MOLLI measurements. Moreover, T1 and T2 values are dependent on the scanner, sequence, sequence variants, and magnetic field strength. Standardization of both data acquisition and analysis is required to ensure a successful transition of mapping techniques into clinical practice (31), and more studies are needed to establish normal reference values and to assess the reproducibility of mapping techniques at different imaging centers and with different scanners.

In conclusion, tissue alterations in liver composition due to fatty infiltration can be objectively quantified using native T1 mapping. In addition to conventional MRI findings, increases in T1 relaxation time can contribute to the assessment of pathologi-

cal tissue changes in NAFLD. To what extent hepatic T1 mapping could influence clinical decision-making compared to currently available fat quantification MRI techniques such as complex-based methods and MRS remains to be investigated. At this stage, additional studies with sufficient sample sizes of NAFLD subgroups are needed to correlate T1 values with histological scoring systems. Also, further research would be of particular value in establishing the use of mapping techniques to monitor treatment strategies.

Conflict of interest disclosure

The authors declared no conflicts of interest.

References

1. Estes C, Razavi H, Loomba R, Younossi Z, Sanyal AJ. Modeling the epidemic of nonalcoholic fatty liver disease demonstrates an exponential increase in burden of disease. Hepatology 2018; 67:123–133. [Crossref]
2. Matteoni CA, Younossi ZM, Gramlich T, et al. Nonalcoholic fatty liver disease: a spectrum of clinical and pathological severity. Gastroenterology 1999; 116:1413–1419. [Crossref]
3. Adams LA, Lymp JF, St Sauver J, et al. The natural history of nonalcoholic fatty liver disease: a population-based cohort study. Gastroenterology 2005; 129:113–121. [Crossref]
4. Issa D, Patel V, Sanyal A. Future therapy for non-alcoholic fatty liver disease. Liver Int 2018; 38:56–63. [Crossref]
5. Chalasani N, Younossi Z, Lavine JE, et al. The diagnosis and management of nonalcoholic fatty liver disease: practice guidance from the American Association for the Study of Liver Diseases. Hepatology 2018; 67:328–357. [Crossref]
6. Sumida Y, Nakajima A, Itoh Y. Limitations of liver biopsy and noninvasive diagnostic tests for the diagnosis of nonalcoholic fatty liver disease/nonalcoholic steatohepatitis. World J Gastroenterol 2014; 20:475–485. [Crossref]
7. European Association for the Study of the Liver (EASL), European Association for the Study of Diabetes (EASD), European Association for the Study of Obesity (EASO). EASL-EASD-EASO clinical practice guidelines for the management of non-alcoholic fatty liver disease. J Hepatol 2016; 64:1388–1402. [Crossref]
8. Chalasani N, Younossi Z, Lavine JE, et al. The diagnosis and management of non-alcoholic fatty liver disease: practice guideline by the American Association for the Study of Liver Diseases, American College of Gastroenterology, and the American Gastroenterological Association. Hepatology 2012; 55:2005–2023. [Crossref]
9. Reeder SB, Robson PM, Yu H, Shimakawa A, et al. Quantification of hepatic steatosis with MRI: the effects of accurate fat spectral modeling. J Magn Reson Imaging 2009; 29:1332–1339. [Crossref]
10. Tang A, Tan J, Sun M, et al. Nonalcoholic fatty liver disease: MR imaging of liver proton density fat fraction to assess hepatic steatosis. Radiology 2013; 267:422–431. [Crossref]
11. Bannas P, Kramer H, Hernando D, et al. Quantitative magnetic resonance imaging of hepatic steatosis: validation in ex vivo human livers. Hepatology 2015; 62:1444–1455. [Crossref]
12. Bray TJ, Chouhan MD, Punwani S, Bainbridge A, Hall-Craggs MA. Fat fraction mapping using magnetic resonance imaging: insight into pathophysiology. Br J Radiol 2018; 91:20170344. [Crossref]
13. Caussy C, Reeder SB, Sirlin CB, Loomba R. Noninvasive, quantitative assessment of liver fat by MRI-PDFF as an endpoint in NASH trials. Hepatology 2018; 68:763–772. [Crossref]
14. Pavlides M, Banerjee R, Tunnicliffe EM, et al. Multiparametric magnetic resonance imaging for the assessment of non-alcoholic fatty liver disease severity. Liver Int 2017; 37:1065–1073. [Crossref]
15. Guimaraes AR, Siqueira L, Uppal R, et al. Quant Imaging Med Surg 2016; 6:103–114. [Crossref]
16. Park C, Nguyen P, Hernandez C, et al. Magnetic resonance elastography vs transient elastography in detection of fibrosis and noninvasive measurement of steatosis in patients with biopsy-proven nonalcoholic fatty liver disease. Gastroenterology 2017; 152:598–607. [Crossref]
17. Imajo K, Kessoku T, Honda Y, et al. Magnetic resonance imaging more accurately classifies steatosis and fibrosis in patients with nonalcoholic fatty liver disease than transient elastography. Gastroenterology 2016; 150:626–637.[Crossref]
18. Costa-Silva L, Ferolla SM, Lima AS, Vidigal PVT, Ferrari TCA. MR elastography is effective for the non-invasive evaluation of fibrosis and necroinflammatory activity in patients with nonalcoholic fatty liver disease. Eur J Radiol 2018; 98:82–89. [Crossref]
19. Loomba R, Wolfson T, Ang B, et al. Magnetic resonance elastography predicts advanced fibrosis in patients with nonalcoholic fatty liver disease: a prospective study. Hepatology 2014; 60:1920–1928. [Crossref]
20. Loomba R, Cui J, Wolfson T, et al. Novel 3D magnetic resonance elastography for the noninvasive diagnosis of advanced fibrosis in NAFLD: a prospective study. Am J Gastroenterol 2016; 111:986–994. [Crossref]
21. Besutti G, Valenti L, Ligabue G, et al. Accuracy of imaging methods for steatohepatitis diagnosis in non-alcoholic fatty liver disease patients: A systematic review. Liver Int 2019; 39:1521–1534. [Crossref]
22. McPherson S, Jonsson JR, Cowin GJ, et al. Magnetic resonance imaging and spectroscopy accurately estimate the severity of steatosis provided the stage of fibrosis is considered. J Hepatol 2009; 51:389–397. [Crossref]
23. Puntmann VO, Carr-White G, Jabbour A, et al. International T1 Multicentre CMR Outcome Study. Native T1 and ECV of noninfarcted myocardium and outcome in patients with coronary artery disease. J Am Coll Cardiol 2018; 71:766–778. [Crossref]
24. Piechnik SK, Ferreira VM, Dall'Armellina E, et al. Shortened modified look-locker inversion recovery (ShMOLLI) for clinical myocardial T1-mapping at 1.5 and 3 T within a 9 heartbeat breathhold. J Cardiovasc Magn Reson 2010; 12:69. [Crossref]
25. Puntmann VO, Carr-White G, Jabbour A, et al. T1-mapping and outcome in nonischemic cardiomyopathy: all-cause mortality and heart failure. ACC Cardiovasc Imaging 2016; 9:40–50. [Crossref]
26. Reeder SB, Cruite I, Hamilton G, Sirlin CB. Quantitative assessment of liver fat with Magnetic Resonance Imaging and Spectroscopy. J Magn Reson Imaging 2011; 34:729–749. [Crossref]
27. Tang A, Desai A, Hamilton G, et al. Accuracy of MR imaging-estimated proton density fat fraction for classification of dichotomized histologic steatosis grades in nonalcoholic fatty liver disease. Radiology 2015; 274:416–425. [Crossref]
28. Obmann VC, Mertineit N, Marx C, et al. Liver MR relaxometry at 3T - segmental normal T1 and T2* values in patients without focal or diffuse liver disease and in patients with increased liver fat and elevated liver stiffness. Sci Rep 2019; 30:8106. [Crossref]
29. Mozes FE, Tunnicliffe EM, Pavlides M, Robson MD. Influence of fat on liver T1 measurements using modified Look-Locker inversion recovery (MOLLI) methods at 3T. J Magn Reson Imaging 2016; 44:105–111. [Crossref]
30. Mozes FE, Tunnicliffe EM, Moolla A, et al. Mapping tissue water T1 in the liver using the MOLLI T1 method in the presence of fat, iron and B0 inhomogeneity. NMR Biomed 2019; 32:4030. [Crossref]
31. Taylor AJ, Salerno M, Dharmakumar R, Jerosch-Herold M. T1 mapping: basic techniques and clinical applications. JACC Cardiovasc Imaging 2016; 9:67–81. [Crossref]
32. Chen J, Talwalkar JA, Yin M, Glaser KJ, Sanderson SO, Ehman RL. Early detection of nonalcoholic steatohepatitis in patients with nonalcoholic fatty liver disease by using MRE. Radiology 2011; 259:749–756. [Crossref]
33. Hardy T, McPherson S. Imaging-based assessment of steatosis, inflammation and fibrosis in NAFLD. Curr Hepatol Rep 2017; 16:298–307. [Crossref]
34. Thiesson SB, Thompson RB, Chow K. Characterization of T1 bias from lipids in MOLLI and SASHA pulse sequences. JCMR 2015; 17:W10. [Crossref]
35. Kellman P, Bandettini WP, Mancini C, Hammer-Hansen S, Hansen MS, Arai AE. Characterization of myocardial T1- mapping bias caused by intramyocardial fat in inversion recovery and saturation recovery techniques. J Cardiovasc Magn Reson 2015; 17:33. [Crossref]
36. Chow AM, Gao DS, Fan SJ, et al. Measurement of liver T_1 and T_2 relaxation times in an experimental mouse model of liver fibrosis. J Magn Reson Imaging 2012; 36:152–158. [Crossref]
37. Wilman H, Bachtiar V, Jacobs J, et al. Repeatability and reproducibility of multiparametric magnetic resonance imaging of the liver. J Hepatol 2018; 68:S562 (Abstract FRI-443). [Crossref]
38. Kleiner DE, Brunt EM, Van Natta M, et al. Nonalcoholic steatohepatitis clinical research network. Design and validation of a histological scoring system for nonalcoholic fatty liver disease. Hepatology 2005; 41:1313–1321. [Crossref]
39. Reiter G, Reiter C, Kräuter C, Fuchsjäger M, Reiter U. Cardiac magnetic resonance T1 mapping. Part 1: aspects of acquisition and evaluation. Eur J Radiol 2018; 109:223–234. [Crossref]
40. Dekkers IA, Lamb HJ. Clinical application and technical considerations of T1 &T2(*) mapping in cardiac, liver, and renal imaging. Br J Radiol 2018; 91:20170825. [Crossref]